Composite Structures 393 (2026) 120608

Contents lists available at ScienceDirect

Composite Structures

journal homepage: www.elsevier.com/locate/compstruct

Architecture-stiffness relationships in woven engineered prepreg platelet composites in a closed-section geometry

Alessandro Masetti Placci [a,c,*], Luca Bernini [a,b], Paolo Albertelli [a,b]

[a] Politecnico di Milano, Department of Mechanical Engineering, via La Masa, 1, Milan, 20156, Lombardy, Italy
[b] MUSP Macchine Utensili Sistemi di Produzione, strada della Torre della Razza, Piacenza, 29122, Emilia-Romagna, Italy
[c] Racing Bulls S.p.A, Via Boaria 229, Faenza, 48018, Emilia-Romagna, Italy

ARTICLE INFO

Keywords:
Woven prepreg platelets
Carbon fibre
Discontinuous reinforcement
Stiffness case study

ABSTRACT

This work presents engineered prepreg platelet (EPP) laminates, which consist of architected platelet-based composites with tailorable morphologies. Although many platelet systems are still validated at specimen scale, this work evaluates a closed-section component geometry reinforced with different woven EPP architectures to characterise their impact at component scale stiffness and the transferability of platelet-array computational modelling. A closed-section wing component was manufactured utilising a continuous woven baseline laminate and three EPP architectures, which was then tested in a cantilever bending load test with spanwise displacement measured using displacement transducers. A linear-elastic ABAQUS model was also implemented to capture pre-damage load transfer and validate existing platelet-based modelling techniques and their suitability for component geometries. All EPP architectures exhibit increased deflections between 9 and 13% relative to the continuous laminate, with architecture-dependent stiffness retention remaining consistent with the platelet parameters and overlap-controlled shear transfer. This work demonstrates the potential of woven EPP architectures, and their potential to be tailored according to structural design requirements.

1. Introduction

The widespread adoption of Carbon Fibre Reinforced Polymer (CFRP) composites across aerospace, automotive, renewable energy, and other high-performance sectors is driven by their favourable combination of low density and high specific stiffness and strength [1,2]. In such applications, structural CFRP components are still predominately manufactured from continuous fibre reinforcements, commonly in the form of pre-impregnated carbon fibres consolidated with a partially cured thermoset polymer matrix, termed *prepreg*. Prepreg materials remain widely utilised due to their controlled thickness, fibre volume fraction, and areal weight, alongside their repeatable manufacturing route. However, their growing industrial demand has intensified manufacturing waste streams, particularly through uncured prepreg offcuts generated by nesting inefficiencies, trimming operations, and lay-up constraints [3–5]. In response, significant research effort has been directed towards discontinuous prepreg composite systems that can retain a significant proportion of conventional CFRP performance while improving material utilisation and architectural flexibility.

Platelet-based prepreg composites, also referred to as flakes, chips, patches, strands, or tows [6–11], are particularly advantageous, occupying an intermediate design space between conventional continuous fibre laminates and low performing short-fibre (SF) moulding compounds, with reinforcement architectures that can be explicitly tailored. By controlling platelet dimensions, overlap, placement, and the stacking sequence, platelet-based systems provide a route to engineered discontinuous laminates whose structural response is governed by the material architecture rather than by reinforcement presence alone. The present work denotes this class of materials as *engineered prepreg platelet* (EPP) composites, emphasising the designed and repeatable nature of the platelet morphology, and its distinction from the broader Discontinuous Carbon Fibre Composites (DCFCs) [12] or process-defined terminology such as Prepreg Platelet Moulded Composite (PPMC) [8,9,13]. For EPP systems, analogous to two-dimensional Brick-and-Mortar (BaM) architectures [14], the architectural variables include platelet length, platelet width, longitudinal superposition, transverse superposition, and laminate thickness, Fig. 1.

Given their potential, platelet-based composite systems have been extensively researched to characterise their mechanical behaviour, identify influential architectural parameters, and develop predictive modelling strategies. However, the literature remains dominated by Unidirectional (UD) platelet systems, with most experimental validation being performed at specimen scale under uniaxial or flexural loading [15–17]. As summarised in Table 1, the prevailing focus has been

* Corresponding author at: Politecnico di Milano, Department of Mechanical Engineering, via La Masa, 1, Milan, 20156, Lombardy, Italy.
E-mail addresses: alessandro.masetti@polimi.it (A. Masetti Placci), luca1.bernini@polimi.it (L. Bernini), paolo.albertelli@polimi.it (P. Albertelli).

https://doi.org/10.1016/j.compstruct.2026.120608
Received 22 March 2026; Received in revised form 27 May 2026; Accepted 30 June 2026
Available online 13 July 2026

Table 1
Summary of platelet-based CFRP composites studies with modelling strategies, highlighting the prepreg material system, platelet dimensions tested, morphology (including quasi-isotropic (QI) or Brick-and-Mortar (BaM) lamination), modelling strategy, and validation outcomes of the modelling strategies.

Reference –	Material system –	Platelet dimensions ($l \times w \times t$) [mm]	Morphology –	Scale –	Modelling strategy –	Validation outcome –
[19]	Pyrofil$_{TM}$ MR70 12P CFRP Tape	40 × 20 × 0.0214	Random	Specimen	Analytical shear -lag model [14]	Tensile stiffness and strength
[20]	AS4/PEKK UD Prepreg Tape	12.7 × 12.7 × 0.14 12.7 × 3.175 × 0.12	QI BaM	Specimen	Progressive failure analysis with finite element modelling	Tensile stiffness and strength
[8]	AS4/PEKK UD Prepreg Tape	50.8 × 12.7 × 0.14 25.4 × 12.7 × 0.14 12.7 × 12.7 × 0.14 6.35 × 12.7 × 0.14	UD BaM	Specimen	Progressive failure analysis with finite element modelling	Tensile stiffness and strength
[9]	AS4/PEKK UD Prepreg Tape	12.7 × 12.7 × 0.14	QI BaM	Specimen	Progressive failure analysis with finite element modelling	Tensile stiffness and strength
[21]	T700S/#2500 UD	25 × 12.5 × 0.146	Coincident	Specimen	Analytical fracture mechanics model	Tensile strength
		25 × 12.5 × 0.146 25 × 12.5 × 0.146 25 × 12.5 × 0.146 25 × 12.5 × 0.145 25 × 12.5 × 0.145 25 × 12.5 × 0.119 25 × 12.5 × 0.193 25 × 12.5 × 0.291	UD BaM	Specimen		
		25 × 6.25 × 0.193 25 × 12.5 × 0.197 25 × 25 × 0.190 25 × 50 × 0.194 25 × 25 × 0.047 25 × 25 × 0.093 25 × 25 × 0.123 25 × 25 × 0.243	QI BaM	Specimen	None	None

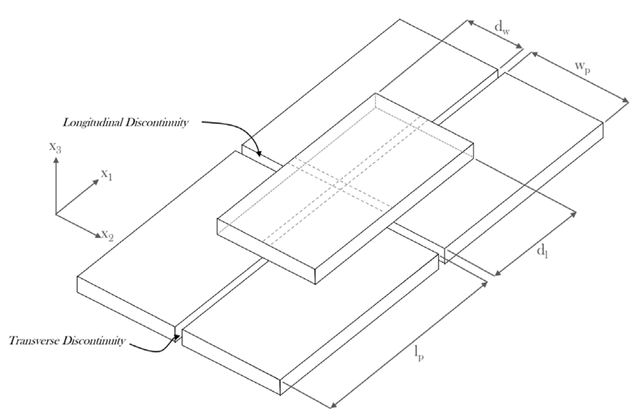

Fig. 1. Schematic illustrating a platelet overlap configuration, denoting platelet length (l_p), platelet width (w_p), longitudinal superposition (δl), transverse superposition (δw), and number of plies (n_p).

on specimen-level tensile properties, often interpreted through analytical shear-lag, fracture mechanics, or Finite Element (FE) platelet-array models. This emphasis is practical, as UD platelet systems maximise on-axis properties and permit comparatively direct stress-transfer descriptions that map well with conventional laminate idealisation, where the platelet meso-scale governs the emergent composite properties [18].

The studies summarised in Table 1 establish the mechanical relevance of platelet length, overlap, and meso-scale morphology for discontinuous prepreg systems. However, they also highlight two limitations in the current state of the art. First, most validated modelling and experimental frameworks are based on UD platelet systems, where load transfer is dominated by the development of axial stress along the platelet length with interlaminar shear transfer across the overlap regions. Second, the majority of validation remains at specimen scale, where the response is governed by simpler tensile or flexural load paths. Consequently, the existing literature provides limited evidence on whether platelet-array modelling approaches remain valid when the material reinforcement is extended woven prepreg systems and embedded in a component.

However, woven prepregs introduce a broader architectural freedom. Unlike UD reinforcements, woven fabrics carry load through two principal fibre directions and are widely utilised in high-performance applications due to their balanced in-plane properties, handling robustness, and improved conformability to complex geometries relative to UD laminates [22,23]. When such reinforcements are converted into engineered platelets, the architecture is no longer only defined by platelet length or longitudinal overlap, but also by platelet width and transverse superposition. These additional degrees of freedom enable a more complete interpretation of platelet aspect ratio and complex load transfer. Nonetheless, these cannot be meaningfully researched through conventional uniaxial specimen testing alone, and as a result, woven EPPs remain under-represented in the literature despite their practical relevance and distinct architecture-property relationships.

This motivates the need to characterise the structure–property relationships introduced by woven CFRP reinforcements by moving beyond specimen-scale validation towards a structural configuration where transverse platelet variables can influence the measured response alongside the longitudinal variables. In this context, a closed-section component is particularly relevant. In addition to representing a stiffness-critical structural form widely encountered in lightweight composite design, a closed-section geometry constrains the development of free-edge and surface-layer peeling effects that are commonly problematic for platelet-based composite systems. This enables a clearer interpretation of the architecture-dependent stiffness response, and such a configuration also provides a more appropriate experimental basis for assessing how woven platelet dimensions and superposition patterns influence the global structural compliance.

This also poses a methodological question concerning predictive design capability. If woven EPP architectures are to be selected and optimised prior to manufacturing, modelling strategies must remain informative and applicable beyond the UD specimen-scale conditions for which they were originally developed. The majority of existing platelet-array FE frameworks have been derived for UD platelet arrays, typically under uniaxial tensile loading with idealised meso-scale morphologies. It therefore remains unclear whether these FE idealisations can be transferred to woven EPP structures, at least within the elastic regime where stiffness remains the primary design metric. This question is particularly pertinent for stiffness-limited structures, where early architecture selection relies on stiffness as the primary property for material suitability [24].

Accordingly, this work presents an experimental and numerical investigation of woven EPPs in a closed-section geometry representative of a stiffness-critical structure. A wing section was selected as the test vehicle and manufactured in collaboration with Racing Bulls S.p.A. [25], implementing three controlled woven EPP architectures produced using scored-and-cut discontinuities for repeatable platelet morphologies. These architectures were benchmarked against an equivalent continuous woven laminate baseline. Structural stiffness was quantified through spanwise deflection profiles under cantilever loading using multiple displacement transducers within an elastic loading regime. In parallel, a linear-elastic FE model was developed by adapting the platelet-array modelling approach reported by Kravchenko et al. [8,9] in order to isolate the pre-damage stiffness response.

The study examines how woven-specific transverse architecture variables influence component stiffness through transverse discontinuity density, bonded overlap area, and resulting inter-platelet shear-transfer efficiency and whether UD-derived platelet modelling strategies can capture both the global compliance and architecture-dependent stiffness ranking of woven EPPs for a component-scale closed-section structure. Ultimately providing a controlled component-scale demonstrator for comparing architecture-dependent stiffness trends alongside computational model validation.

The work is structured as follows. Section 2 describes the methodological approach for the experimental work (Section 2.1) and computational model (Section 2.2). The experimental and numerical results are presented in Section 3, while Section 4 discusses the observed stiffness trends and sources of model and experiment deviations, and Section 5 summarises the key findings.

2. Materials and methods

2.1. Experimental methodology

A closed-section wing geometry was selected as the demonstrator component as it provided a readily available and well-characterised mould platform with an established manufacturing procedure by Racing Bulls S.p.A. The use of an existing tool enabled the study to focus on its primary objective, the assessment of the component-level stiffness response of various EPP architectures and the applicability of tailored woven EPP laminate architectures, rather than optimising the external geometry itself.

2.1.1. Laminate architectures

The material used in this study is a woven CFRP prepreg consisting of $M46J$ carbon fibre reinforcements and a $ER450$ thermoset epoxy resin, with an areal weight of $200\,g/m^2$ produced by Composite Materials Italy (CIT) [26]. This 2 × 2 twill high modulus fabric has a cured ply thickness of 0.22 mm, fibre volume fraction of 60% wt., and was supplied by Racing Bulls S.p.A [25].

The elastic modulus is frequently utilised as a baseline screening property for engineering practise where the structures are stiffness limited [24,25]. An investigation regarding the influence of engineered discontinuity parameters on the tensile behaviour of woven EPPs was carried out, with a Design of Experiments (DoE) that was conceived in order to evaluate the effect of different platelet architectures and their effect on the mechanical performances of the final material. The DoE utilised five different parameters, illustrated in Fig. 1, and were defined to allow modular platelet configurations. The tensile testing therefore provided mechanical performance data representative of the final composite material.

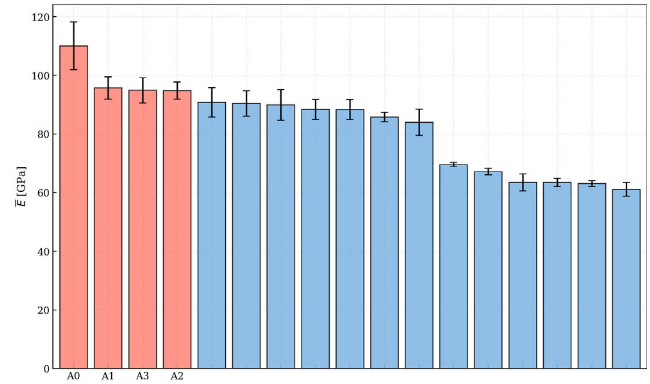

Fig. 2. 4-ply uniaxial tensile test illustrating the Young's Modulus $\overline{E}$ [GPa] of various woven EPP architectures.

Table 2
Summary of the three woven EPP platelet architectures selected for the component-level investigation.

Architecture	l_p [mm]	w_p [mm]	δl [%]	δw [%]	n_p [#]	E [GPa]
A0	–	–	–	–	4	110.1
A1	34.5	45.0	25	50	4	95.7
A2	34.5	15.0	25	25	4	94.4
A3	34.5	15.0	25	50	4	94.9

- l_p, platelet lengths of 34.5, 27.6, and 23.0 mm.
- w_p, platelet widths of 45.0, 15.0 and 22.5 mm.
- δl, platelet longitudinal (length) superposition of 50%, 25% and 33% of the platelet length.
- δw, platelet transverse (width) superposition of 50%, 25% and 33% of the platelet width.
- n_p, number of plies for an EPP architecture of 4, 6, and 8.

The number of plies, n_p, was constrained by the closed-mould geometry, and was limited to four plies. Accommodating these manufacturing constraints, three platelet architectures were chosen from the tested experimental campaign, illustrated in Fig. 2, which exhibited the highest Young's Modulus (E) retention with varying platelet width and transverse superpositions. The architectures are illustrated in Fig. 3 and summarised in Table 2. Due to the component-scale nature of the investigation and the manufacturing constraints associated with the closed-section geometry, only one component was manufactured and tested for each reported architecture. The experimental campaign therefore consisted of four components, of which one constituted the woven laminate baseline (A0) and one specimen for each selected EPP architecture (A1–A3).

The selected EPP architectures exhibited a characteristic composite stress–strain response during their tensile testing, Fig. 4. Each specimen demonstrating a linear-elastic regime followed by an abrupt and brittle failure, with no evidence of ply-by-ply damage failure or pseudo-ductility. This motivated the focus on a linear-elastic model for the component-level analysis.

2.1.2. Geometry manufacturing

The components were manufactured by Racing Bulls S.p.A. [25] at their facility in Faenza, Italy. To achieve precise and repeatable

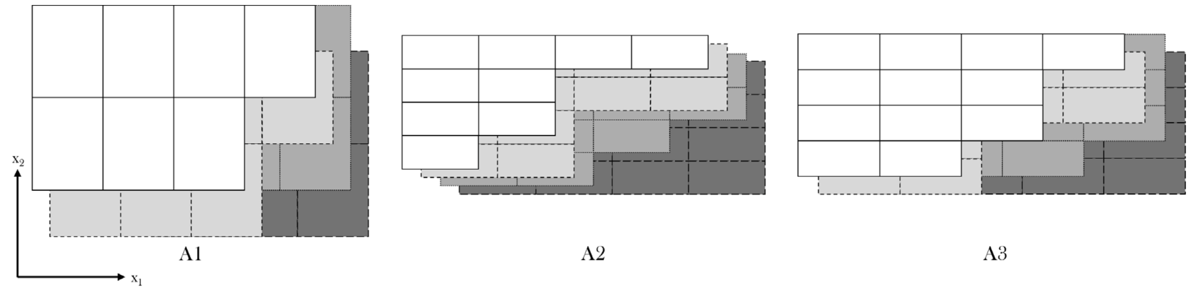

Fig. 3. Schematic of the tested EPP architectures.

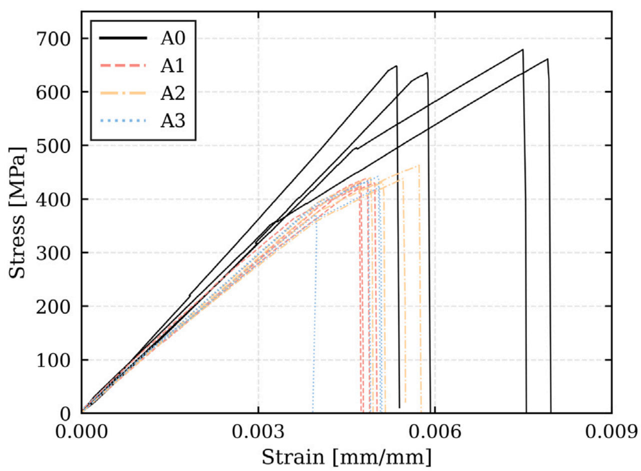

Fig. 4. Tensile stress–strain curves of all tested laminate architectures.

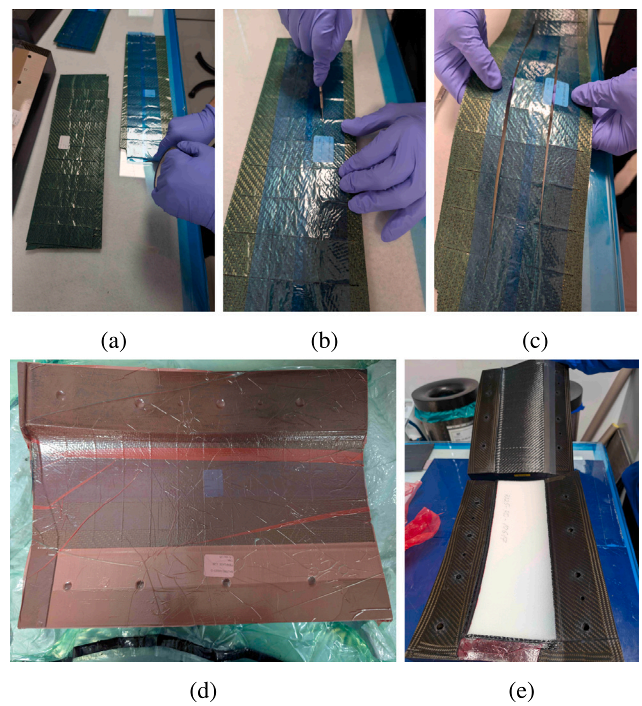

Fig. 5. Specimen manufacturing process (courtesy of Racing Bulls S.p.A [25]) (a) Cut and scored geometry plies from plotter (b) Taping of release film on prepreg ply prior to cutting the scored platelet discontinuities (c) Resulting platelet discontinuities prior to lamination on mould (d) De-bulking process for the first ply on one of the mould halves (e) Positioned insert and core on one mould half.

platelet arrangements while simplifying the lay-up procedure and minimising alignment-related manufacturing defects, an automated ply cutter (plotter) was used. Precursor woven prepreg plies were cut from a prepreg roll to the net ply shape. The plotter also cut and scored the platelet discontinuities on the prepreg fabric, Fig. 5a. This approach preserved the ply's homogeneity, allowing for easier handling while controlling the platelet discontinuities, maintaining consistency between plies.

The remaining scored platelet discontinuities on the nested plies were hand cut prior to lamination, Fig. 5b, using tape to retain the integrity of the nested plies, 5c. The first ply was subsequently positioned on the mould and de-bulked under vacuum to remove entrapped air and to compact the lamina against the mould, Fig. 5d. Once the lay-up was completed on either mould half, the core and inserts were positioned on one of the mould halves prior to their assembly, Fig. 5e. A CFRP insert was incorporated to provide a robust interface for the bolts mounting the component to the mounting blocks. Additionally, a Rohacell foam core [27] was wrapped with reinforcing cleats to support the closed-section geometry, Fig. 5e.

The mould was closed using carbon spars on both ends and prepared for autoclave processing. The assembly was covered with breather cloth, vacuum bagged, and vacuum-sealed [25]. The components were subsequently placed in an autoclave with the following cure cycle. Initially the temperature increased to 135 °C at a rate of 2 °C/min as the pressure increased to ∼6 bar at a rate of 0.3 bar/min. This temperature and pressure were maintained for two hours, after which the mould was allowed to cool under pressure to 35 °C at a rate of 3 °C/min. The pressure subsequently dropped at a rate of 0.3 bar/min to atmospheric. The cycle is represented in Fig. 6.

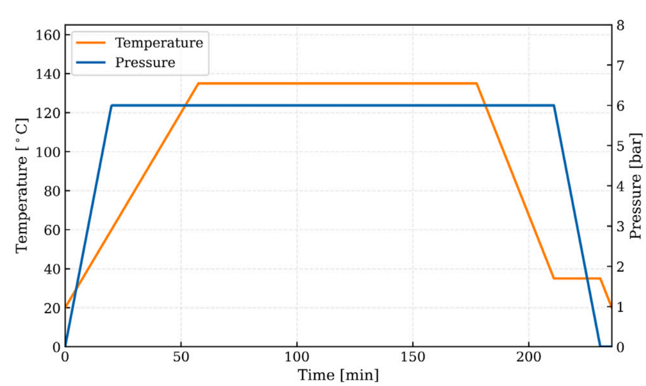

Fig. 6. Graph illustrating the pressure and temperatures of the cure cycle for the production of specimens.

2.1.3. Experimental test setup

A custom test-bench configuration was developed to apply a cantilever boundary condition to the closed wing geometry, Fig. 7a. The

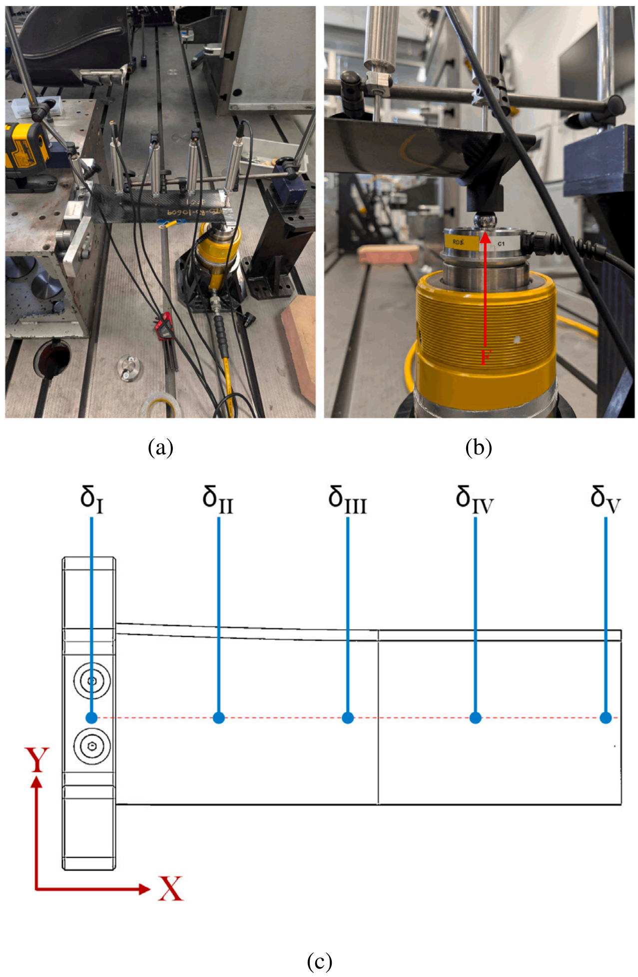

Fig. 7. Experimental test setup (courtesy of Racing Bulls S.p.A [25]) (a) Custom experimental test configuration showing the integrated load cell and load-applicator block, the fixed mounting plate and linear displacement transducers (b) Custom load-applicator block (c) Schematic of displacement transducer locations along the wing component.

geometry was bonded to two aluminium mounting blocks using a two-part structural adhesive, $3M^{®}$ 9323 [28], after which it was mechanically fastened using $M10$ shoulder bolts to minimise slip or de-bonding and to ensure a repeatable clamped-end condition. This bonded assembly was mounted to the rigid back plate of the test apparatus.

External loading was applied through a dedicated load-applicator block, Fig. 7b, which interfaces with the component through a defined surface area to distribute the applied force over a finite contact region. The applied load was measured through the load cell supplied by Racing Bulls S.p.A [25] (Fig. 7b). Load and displacement data were acquired using proprietary software developed through LabVIEW [29], which synchronously recorded the load applied and the output displacements from the linear transducers to the same time step. A target load of 700 N was adopted to ensure the response remained within the elastic regime and to prevent damage initiation that could influence the measured stiffness. The load was applied incrementally under quasi-static conditions, without prescribing a constant loading rate.

To compare the overall structural response of the components, the vertical displacement of each component was measured using five contact displacement transducers, AEP linear displacement transducers [30], sampled at 1600 Hz. The transducers were aligned along a centreline which is perpendicular to both the fixed mounting plate and the load cell, while also being parallel to the loading axis. The nominal positions of the transducers from the mounting plate were: $x = 23.00$ mm, $\times 121.25$ mm, 219.50 mm, 317.75 mm, 416.00 mm corresponding to δ_{I-V}, respectively, Fig. 7c. The last transducer (δ_V) was positioned directly over the load cell, aligned with the load vector.

The instrumental uncertainty was taken as the reported accuracy for the AEP transducers, $\pm 0.10\%$ of the recorded displacement. Since only one component was tested for each architecture, the reported uncertainty bounds correspond to measurement uncertainty only and do not represent specimen-to-specimen manufacturing scatter.

2.2. Computational modelling

The composite system considered in this work comprises an array of discontinuous woven CFRP prepreg platelets arranged in a controlled and repeatable morphology. Each layer consists of platelets placed side-by-side and nominally parallel, with adjacent layers being staggered in the local longitudinal and transverse directions to form a periodic overlapping pattern, idealised in Fig. 1.

2.2.1. Meso-scale stress state in woven platelet architectures

For the present linear-elastic analysis, the woven platelet architecture is idealised as a regular and repeating array of discrete platelets separated by a finite lateral spacing, Δ_s, such that each platelet is bonded to neighbouring platelets through the upper and lower interfaces. The longitudinal and transverse superpositions considered are 50%, providing a symmetric overlap arrangement for both in-plane directions and ensuring that neighbouring bonded regions have the same nominal area, Fig. 1. The imposed spacing Δ_s preserves the discrete nature of the platelet system, resulting in finite unbonded regions along the platelet length and width, which define the local discontinuities governing stress transfer.

Unlike UD platelet arrays, woven platelets can support load through two principal reinforcement directions, and the local stress states are therefore described by a coupled stress-transfer along both the platelet length and width. Under in-plane loading, axial stresses develop within the platelet along the fibre directions (σ_{11} and σ_{22}), while interfacial load transfer with neighbouring platelets gives rise to the corresponding interlaminar shear stresses (σ_{13} and σ_{23}). For platelets located on the laminate surface, the imbalance of these interfacial shear tractions also generates a local through-thickness normal stress (σ_{33}), associated with peeling effects. The resulting stress distributions along the platelet length and width are shown in Fig. 8.

Stress is transferred between neighbouring platelets through the bonded overlap regions (cohesive interface) with in-plane shear stresses, σ_{13} and σ_{23}, developing at the interface with opposite signs on either side of the discontinuities. This redistribution causes local amplification of the in-plane axial stresses, enhancing σ_{11} and σ_{22} in the discontinuous regions. If the platelets were assumed rigid, the interfacial shear tractions would tend towards a uniform distribution across the overlaps. However, in practice, the platelet compliance causes strain compatibility to vary along the bonded region, minimising at the platelet edges, with corresponding interfacial shear stresses concentrating towards the overlap edges. For internal plies, these interfacial shear stresses are self-equilibrated, while for surface plies, the absence of a balancing stress results in a through-thickness normal stress, σ_{33}, is produced, restricted to a small edge region [31].

The force-balance cases considered in Fig. 9a–h [32] formalise these local equilibrium conditions for representative woven platelet sub-regions. The shaded region in each schematic denotes the platelet element under consideration. The woven platelet architectures can therefore be interpreted as a repeating network of locally unbalanced and re-balanced stress-resultant zones, rather than as a single one-dimensional shear-lag problem.

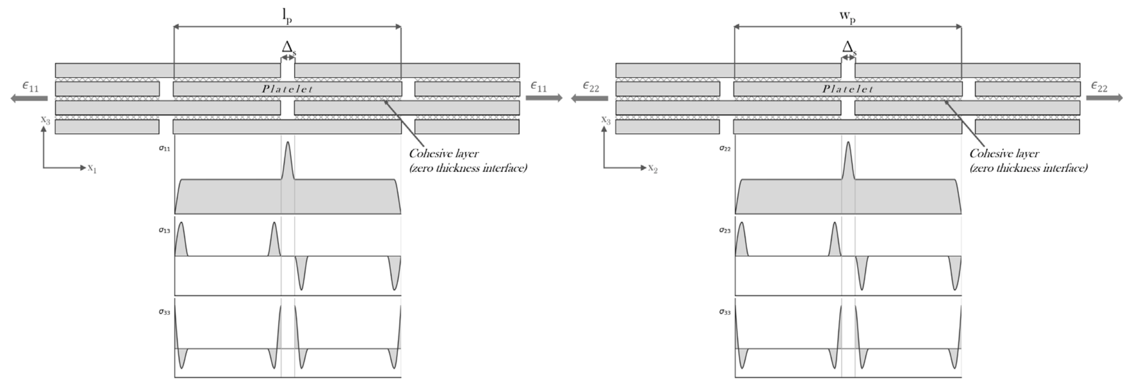

(a) (b)

Fig. 8. Stresses acting along the (a) platelet length (b) platelet width.

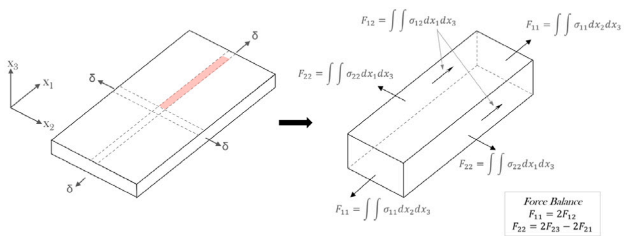

(a) Transverse discontinuity force balance.

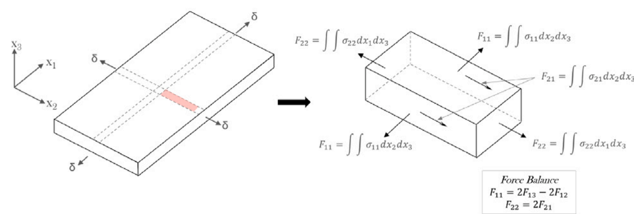

(b) Longitudinal discontinuity force balance.

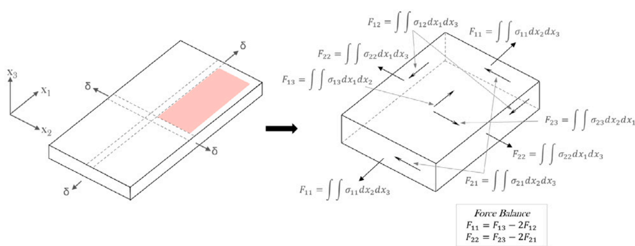

(c) Platelet force balance.

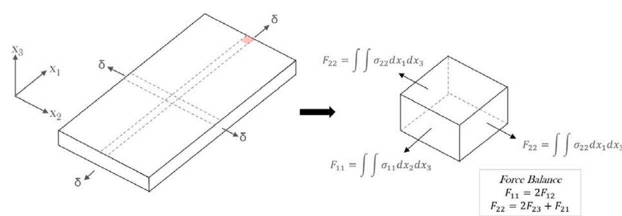

(d) Edge transverse discontinuity force balance.

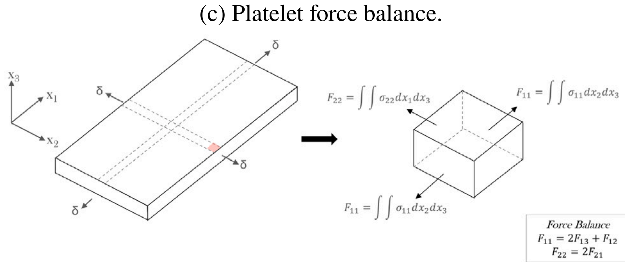

(e) Edge longitudinal discontinuity force balance.

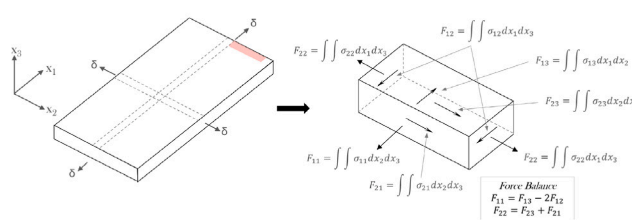

(f) Edge transverse platelet force balance.

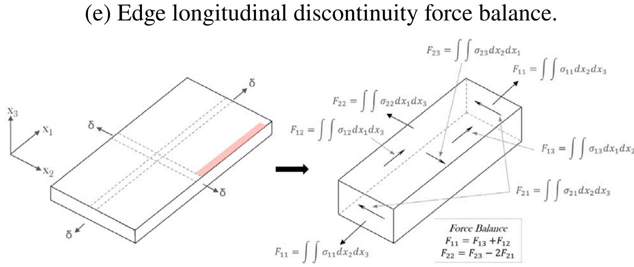

(g) Edge longitudinal platelet force balance.

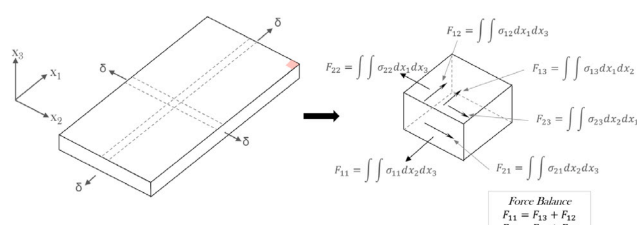

(h) Corner platelet force balance.

Fig. 9. Force Balance within woven platelet elements.

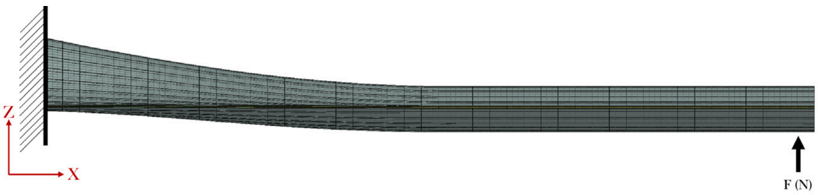

(a)

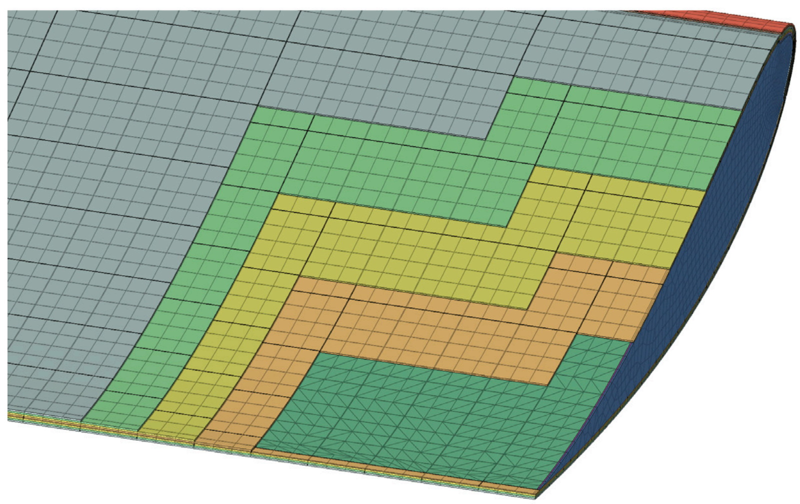

(b)

Fig. 10. Geometry and mesh of the EPPs used in the numerical tests (a) General wing component specimen and schematic of cantilever test (b) Detailed view of the FE mesh showcasing platelet staggering.

2.2.2. Linear-elastic finite element implementation

Based on the preceding stress-transfer interpretation, the woven EPP architecture was represented explicitly as an array of discrete platelets connected through platelet-to-platelet interfaces. The objective of the numerical framework was to reproduce the *pre-damage* redistribution of axial, bending, and interfacial stresses governing the elastic stiffness response, rather than progressive fracture or delamination growth. The modelling philosophy therefore follows the platelet-array approach introduced by Kravchenko et al. [8], with additional guidance from Sommer et al. [9], while adapting the framework to a woven platelet morphology and restricting the analysis to the linear-elastic regime relevant to the experimental component stiffness assessment.

The composite system considered in this work comprises a controlled and repeatable array of discontinuous woven CFRP prepreg platelets. Within each layer, platelets are positioned nominally parallel and side-by-side, with subsequent layers being staggered in the local width and length directions to produce the engineered overlap pattern shown in Fig. 10b. All analyses were carried out in ABAQUS/Standard [33], with pre-processing and meshing being conducted in Altair HyperMesh [34].

Platelet geometry and discretisation. The platelets were discretised using reduced-integration continuum shell elements (SC8R/SC6R). This formulation is appropriate because the platelet thickness is much smaller than the in-plane dimensions ($t_p \ll l_p, w_p$), allowing the orthotropic lamina response and finite platelet thickness to be retained while remaining computationally efficient at a component scale. Although continuum shell elements are geometrically six- or eight-noded solid-like elements, they employ a plane-stress formulation, behaving as a shell and enabling computational efficiency while retaining the essential stress transfer through the interfaces.

The local material axes for each continuum-shell platelet were assigned using the nominal fabric directions, with the *1* and *2* directions aligned with the warp and weft directions of the woven prepreg, respectively. The homogenised mechanical properties used for the woven composite platelets are given in Table 3.

Table 3
Material properties for $M46J/ER450$ carbon fibre epoxy resin CFRP used in the computational analysis [26].

Material properties	$M46J/ER450$
Longitudinal modulus, E_{11} [GPa]	110.1
Transverse modulus, E_{22} [GPa]	107.4
Shear modulus, G_{12} [GPa]	3.7
Poisson's ratio, ν_{12}	0.04

It is acknowledged that, for twill weaves, the identification of principal material axes is less direct than for plain weaves as the mesoscopic architecture lacks reflectional symmetry about the warp and weft directions. Meng et al. [35] showed, through material symmetry analysis, that the rotational symmetries of twill woven lamina can nevertheless lead to admissible macroscopic principal axis systems in both the $0°/90°$ and $+45°/-45°$ directions. Therefore, the warp/weft material axis sign adopted here was done to reflect the lamination and used as an effective homogenised lamina approximation for the global stiffness response.

To replicate the experimentally introduced discontinuities between adjacent platelets (Δ_s), a nominal clearance of 100 μm was introduced around each platelet (Fig. 10b). Although these regions are considered matrix-rich inter-ply zones in the manufactured laminates, they were modelled as void spaces in the FE representation. This idealisation reduces geometric and constitutive complexity and ensures that inter-platelet load transfer is governed solely by the defined interface formulation rather than by continuum matrix elements within the incision. The assumption is consistent with the modelling strategies adopted by Kravchenko et al. [8] and Sommer et al. [9].

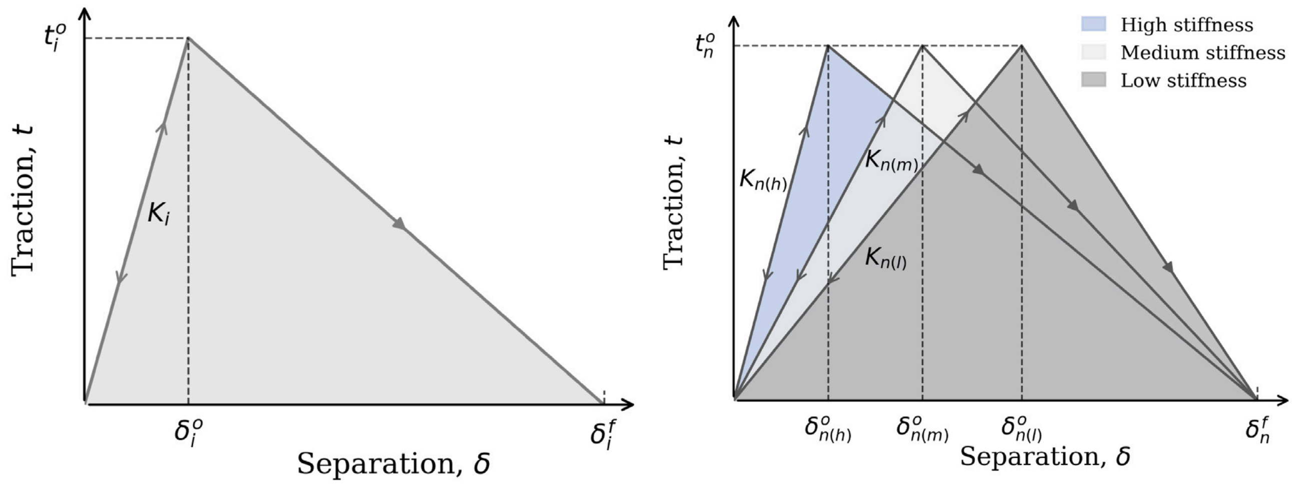

(a) Bilinear traction-separation law.

(b) Bilinear traction-separation law sensitivity to penalty stiffness.

Fig. 11. Schematic representation of the cohesive traction-separation formulation used for the platelet-to-platelet interfaces.

Platelet-to-platelet interfaces. Platelet-platelet load transfer within the overlapping regions was represented using a mixed-mode cohesive-zone formulation governed by a bilinear traction-separation law, implemented natively in ABAQUS [33]. Surface-to-surface contact with frictionless tangential, hard normal, and cohesive behaviours was assigned between the individual layers of platelets. Such contact pairs provide a simplified way to model cohesive connections with negligibly small interface thicknesses by relating the contact/interface tractions, δ_i, to the contact separations, $\delta_i = \Delta u_i$ $(i = 1, 2, 3)$, between the adjacent surfaces:

$$\begin{Bmatrix}\sigma_{13}\\ \sigma_{23}\\ \sigma_{33}\end{Bmatrix} = \begin{bmatrix}(1-d)k_1^0 & 0 & 0\\ * & (1-d)k_2^0 & 0\\ * & * & (1-d)k_3^0\end{bmatrix}\begin{Bmatrix}\delta_1\\ \delta_2\\ \delta_3\end{Bmatrix} \tag{1}$$

where σ_{13} and σ_{23} are the interlaminar shear tractions, σ_{33} is the interlaminar normal traction, δ_i are the corresponding separation components, k_i^0 are the initial elastic cohesive stiffnesses, and d is a scalar damage variable. Although this traction-separation formulation permits stiffness degradation through damage evolution, the present study considers only the linear-elastic regime. Accordingly, the response is restricted to the *pre-damage* stage ($d = 0$), such that the interface behaves as a linear elastic relation between tractions and separations.

Inter-platelet interfaces are often represented as thin matrix layers in the overlap regions. However, for the component geometry tested in this work, the cohesive behaviour was implemented using cohesive surface interactions. A zero initial thickness was implemented rather than discrete cohesive solid elements, consistent with the approach of Sommer et al. [9]. This formulation relates the interface tractions to the corresponding separations through an initial penalty stiffness, as schematically illustrated in Fig. 11a. Since the present analysis is restricted to the linear-elastic regime, only the initial ascending branch of the traction separation law is active.

The initial cohesive stiffness was prescribed uniformly for all separation components as $k_i^0 = k^0 = 7.5 \times 10^5\,\mathrm{N/mm^3}$. This value was selected within the range of stiffness values proposed by Zou et al. [36] for epoxy-based cohesive interfaces, which is between $10^5 \sim 10^7\,\mathrm{N/mm}$ times the shear strength of the matrix. Since the platelet-to-platelet interface stiffness directly controls the elastic shear-transfer path between overlapping platelets, the influence of this parameter was assessed through a sensitivity analysis, discussed in Section 3.3. The effect of varying the initial penalty stiffness is illustrated schematically in Fig. 11b

The component's global stiffness response $\mathbf{K}$ is governed by the continuum shell platelets and cohesive surface interactions, which ABAQUS solves the assembled equilibrium system $\mathbf{K}u = f$ for the applied load and boundary conditions. Component stiffness is therefore evaluated directly from the resulting displacement field by extracting the spanwise deflections at the transducer locations and forming the corresponding stiffness profile $\mathrm{k}(x) = \mathrm{F}/\delta(x)$ at $\mathrm{F} = 700$ N, enabling a like-for-like comparison with the experimental deflection measurements.

Table 4
Summary of the measured deflection values at the displacement transducer locations for the three woven laminate architectures at 700 N load.

Architecture	δ_I [mm]	δ_{II} [mm]	δ_{III} [mm]	δ_{IV} [mm]	δ_V [mm]
A0	0.00	1.29	4.52	8.73	13.85
A1	0.00	1.40	4.94	9.56	15.33
A2	0.00	1.52	5.13	10.07	15.68
A3	0.00	1.41	4.99	9.74	15.10

3. Results

3.1. Experimental results

The experimental deflection response of the closed-section geometries at a target load of 700 N is summarised in Fig. 12. Deflection profiles were constructed from the displacement transducer measurements using a cubic spline interpolation through all measurement points. The dataset includes the baseline continuous laminate (A0) and three woven EPP architectures (A1-A3). The corresponding deflection values at the displacement transducer locations, δ_{I-V}, are reported in Table 4.

Across the wing span, all EPP architectures exhibit increased deflections compared to the continuous laminate baseline, confirming a reduction in effective component stiffness. This increase in deflection is relatively modest near the root and becomes evident towards the free end. At the outermost transducer location (δ_V), the measured deflection increases from 13.85 mm for A0 to 15.10–15.68 mm for A1–A3, corresponding to a 9–13% increase relative to the baseline laminate. Despite this compliance penalty, the EPP architectures retain a deflection profile closely aligned with that of A0, indicating that the introduction of engineered discontinuities primarily reduces the effective bending stiffness for individual platelets without significant stress concentrations altering the deformation. Since the spanwise curves are obtained by cubic-spline interpolation between discrete transducer

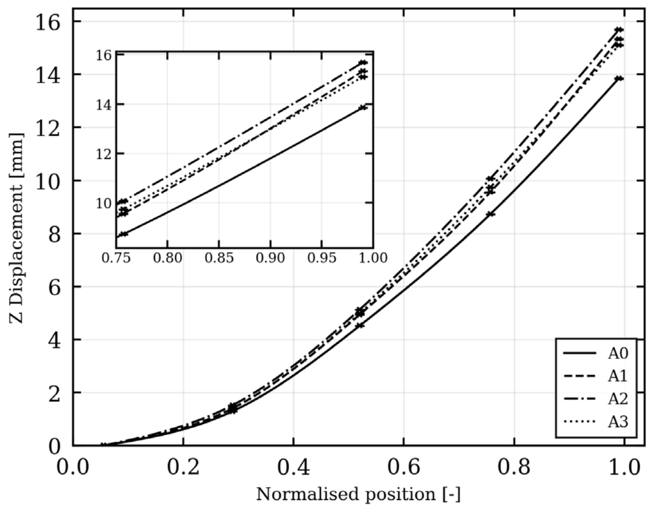

Fig. 12. Comparison of measured deflection profiles for the baseline continuous specimen [A0] and three woven EPP architectures [A1 & A2 & A3] at 700 N load. The uncertainty bounds correspond to the instrumental displacement uncertainty of the displacement transducers.

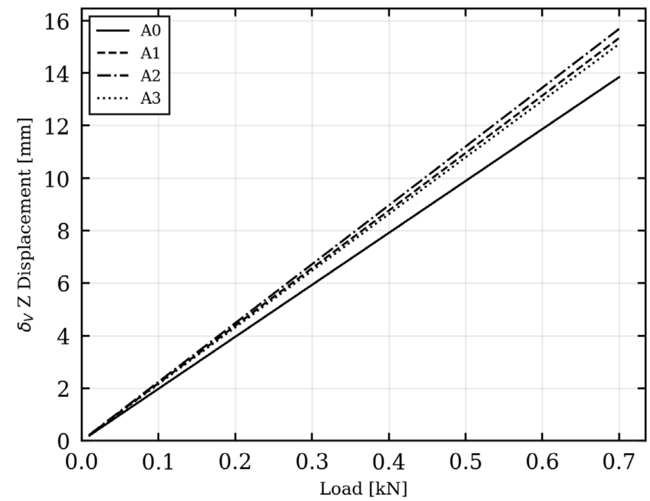

Fig. 13. Experimental load–displacement responses measured at the maximum deflection transducer location, δ_V.

positions, this interpretation is principally supported by the measured values at δ_{I-V} reported in Table 4.

This stiffness reduction can be interpreted through the stress-transfer framework introduced in Section 2.2.1. In the continuous woven laminate, bending loads are carried through an uninterrupted ply, with the warp and weft fibre tows contributing to the in-plane stiffness properties. In woven EPP laminates, this load path is interrupted by longitudinal and transverse platelet discontinuities. Therefore, axial and bending stresses must be transferred from one platelet to neighbouring platelets through the overlap regions, occurring primarily through interlaminar shear stresses, σ_{13} and σ_{23}, with additional through-thickness normal stresses, σ_{33}, developing near platelet edges. Therefore, the measured stiffness response is governed by the intrinsic woven prepreg material properties, but also by the efficiency with which the architecture can reconstruct an approximately continuous load path through shear transfer.

The architecture comparisons provide an indication of the role of the transverse platelet design variables introduced for the woven systems, within the investigated design space. Architectures A1 and A2 share the same platelet length, l_p, and lengthwise superposition, δl, such that the observed difference in response is mainly associated with platelet width, w_p, and widthwise superposition, δw, A1 employs wider platelets ($w_p = 45.0$ mm) and a greater widthwise superposition ($\delta w = 50\%$) than A2 ($w_p = 15.0$ mm, $\delta w = 25\%$, respectively). In the measured response, A1 exhibits lower deflection values than A2 at all measured locations δ_{II-V}. The wider platelets and greater overlap width of A1 reduces the density of transverse discontinuities and the number of platelet-to-platelet transitions across the shell width, promoting a more continuous lateral load-transfer path and therefore a lower global compliance.

The comparison between A2 and A3 was designed to isolate the effect of transverse superposition δw, while holding the remaining architectural parameters constant. Increasing δw from 25% (A2) to 50% (A3) produces a consistent reduction in deflection along the span, indicating a measurable stiffness recovery associated with transverse overlap alone. This behaviour is consistent with the increase in effective bonded area enhancing inter-platelet shear transfer and improving load continuity within the closed-section shell. Although previous studies have indicated that certain overlap combinations may promote local stress concentrations within matrix-rich regions, reducing transfer efficiency [37], no comparable penalty is evident in the present component-scale response. Instead, the increased transverse superposition in A3 results in a net stiffness benefit, indicating that the additional platelet width overlap allows for sufficient stress transfer within the investigated architecture range.

To confirm that all configurations were loaded within a linear-elastic regime, the load–displacement response at the maximum deflection transducer location, δ_V, is shown in Fig. 13.

3.2. Numerical results

The displacement response of the closed-section geometry predicted by the numerical models is compared to the experimental measurements in Fig. 14. To facilitate a direct comparison between experimental and numerical configurations, only the displacement values corresponding to the maximum applied load of 700 N is considered. Numerical displacements corresponding to the transducer locations were extracted by spatially averaging nodal values over regions matching the displacement transducer tip footprint, reducing local nodal scatter and better approximating the finite contact area of the transducers. Meanwhile the deflection curves were extracted from spanwise nodal deflection values.

To account for the variability of the parent woven prepreg properties, the measured material's properties were varied according to the measured standard deviation to produce an additional numerical uncertainty. The resulting bounds provide an estimate of the sensitivity of the predicted deflection response to material-property scatter.

Overall, the model reproduces the measured deflection profiles well. For all architectures, the numerical curves capture the cantilever shape of the displacement distribution and preserve the relative compliance ranking observed experimentally. The detailed displacement values at the transducer locations, and their mean percentage differences to the experimental results are summarised in Table 5.

The numerical model reproduces the measured spanwise deflection response with good agreement across all architectures. The predicted curves capture the cantilever-like deformation profile while preserving the main architecture-dependent stiffness trends observed experimentally. The closest agreement to the experimental values was obtained for A2, while A0 and A1, and A3 exhibited a modest tendency for the numerical predictions to overestimate the deflection values towards the free end of the component.

The continuous baseline laminate, A0, showed good agreement with the experimental response, with a mean difference of 2.92%. The discrepancy increases marginally towards the unconstrained component

Table 5
Summary of the measured deflection values at the displacement transducer locations for continuous woven laminate and the three woven EPP architectures at 700 N load.

Architecture	δ_I [mm]	δ_{II} [mm]	δ_{III} [mm]	δ_{IV} [mm]	δ_V [mm]	Mean δ_i difference [%]	Scatter [%]
A0 Exp.	0.00	1.29	4.52	8.73	13.85		
A0 Num.	0.00	1.28	4.60	9.17	14.51	2.92	2.05
A1 Exp.	0.00	1.40	4.94	9.56	15.33		
A1 Num.	0.00	1.51	5.15	10.06	15.89	5.33	2.09
A2 Exp.	0.00	1.52	5.13	10.07	15.68		
A2 Num.	0.00	1.53	5.20	10.16	15.68	0.82	0.58
A3 Exp.	0.00	1.41	4.99	9.74	15.10		
A3 Num.	0.00	1.48	5.22	10.28	15.83	4.90	0.43

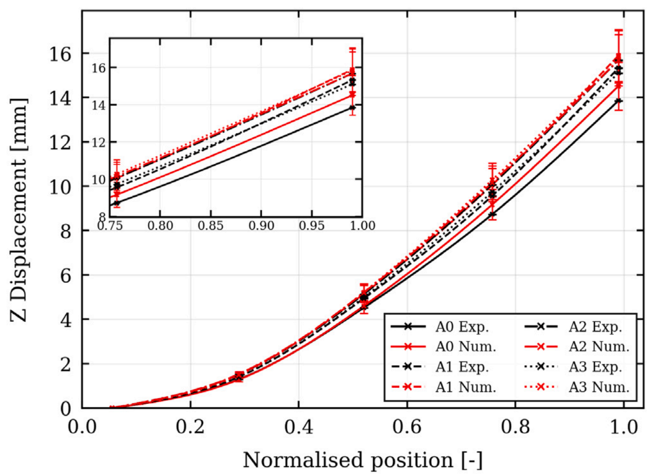

Fig. 14. Comparison of numerically simulated and measured deflection curves for the three woven laminate architectures at 700 N load.

end, where the absolute deflections are largest and any small difference in stiffness representation, boundary conditions, or measurement conditions is amplified at δ_{IV-V}. Meanwhile, the woven EPP architectures show similarly good agreement. For A1, the predicted response follows the experimental curve closely, with a mean difference of 5.33%, although the deviation becomes more evident towards the outer span locations. In contrast, A2 shows the closest correspondence between the numerical and experimental results, with a mean difference of 0.82% and a low scatter of 0.58%. This level of agreement indicates that the platelet-resolved linear-elastic framework is capable of reproducing the stiffness response of a discontinuous woven platelet component with high fidelity. Architecture A3 exhibits a similarly consistent spanwise trend, reflected by the low scatter of 0.43%, but with a greater mean difference of 4.90% to the experimental results. In this case, the numerical response remains approximately parallel to the measured curve, indicating that the model captures the spanwise deformation shape but overestimates the displacement magnitude. This suggests that the discrepancy is associated primarily with absolute compliance. with potential sources for this offset are discussed in Section 4.

Importantly, the numerical model also preserves the experimentally observed stiffness ordering associated with the transverse woven architecture variables. The comparison between A1 and A2 reproduces the lower compliance of the wider, more highly superposed architecture A1, confirming that the model remains sensitive to the in-plane stresses experienced by the platelets with changes in platelet width, w_p, and transverse superposition, δw. Similarly, the comparison between A2 and A3 reproduces the stiffness recovery obtained by increasing δw while retaining all other platelet parameters constant. This demonstrates that the adapted platelet-array framework is not only able to reproduce the global deflection response, but also discriminate between width-controlled architecture effects that arise with woven platelet systems.

Collectively, the comparisons in Fig. 14 and Table 5 show that the linear-elastic FE model captures both the global deformation mode and architecture-dependent stiffness trends for a closed-section component. The model therefore provides a suitable baseline for interpreting the experimentally observed woven platelet behaviour and for future parametric investigations regarding platelet architecture effects.

3.3. Sensitivity study on cohesive stiffness

A sensitivity analysis was performed to evaluate the influence of the platelet-to-platelet cohesive stiffness on the predicted component stiffness response. Although the cohesive interfaces governs the load transfer between overlapping platelets, the selected penalty stiffness should not govern the component's global compliance to the same extent as the architectural parameters and parent material properties. Accordingly, five values of k_i^0 were investigated, spanning the literature-supported interval proposed for epoxy-based cohesive interfaces by Zou et al. [36]. The analysed values were $1.0 \times 10^5, 3.75 \times 10^5, 7.5 \times 10^5, 3.0 \times 10^6$, and 1.0×10^7 N/mm^3, with 7.5×10^5 N/mm^3 corresponding to the reference value used in the computational model.

The resulting deflection profiles are shown in Fig. 15. Across all architectures, reducing the cohesive stiffness nearing the lower literature-bound value increases the predicted deflection, confirming that the platelet-to-platelet interface contributes to the stress-transfer path. However, the sensitivity decreases as k_i^0 increases. For stiffness values equal to or greater than the reference value, the predicted deflection profiles become nearly coincident, indicating that the interface response approaches a stiffness-insensitive regime within the investigated range. This behaviour suggests that the cohesive stiffness affects the predicted component stiffness response when the interface is made comparatively soft and when the stiffness increases beyond the reference value, limited changes in the structural response are observed.

4. Discussion

This section interprets the measured and predicted deflection responses in terms of the architecture-property relationships of woven EPP laminates within a closed-section component geometry. The experimental and numerical responses were quantified through spanwise deflection profiles obtained from displacement transducer measurements under an end-loaded cantilever configuration. The measured load–displacement response at the maximum deflection location, δ_V, shown in Fig. 13, exhibits a linear relationship over the investigated load range, supporting the use of a linear-elastic numerical framework.

A limitation of the experimental campaign is that only one component was manufactured and tested for each architecture. Therefore, the measured deflection differences between architectures cannot be interpreted as statistically validated differences arising from replicated specimens. Instead, the experimental results should be interpreted as a controlled component-scale demonstrator study, where the measured trends are evaluated alongside the known architectural

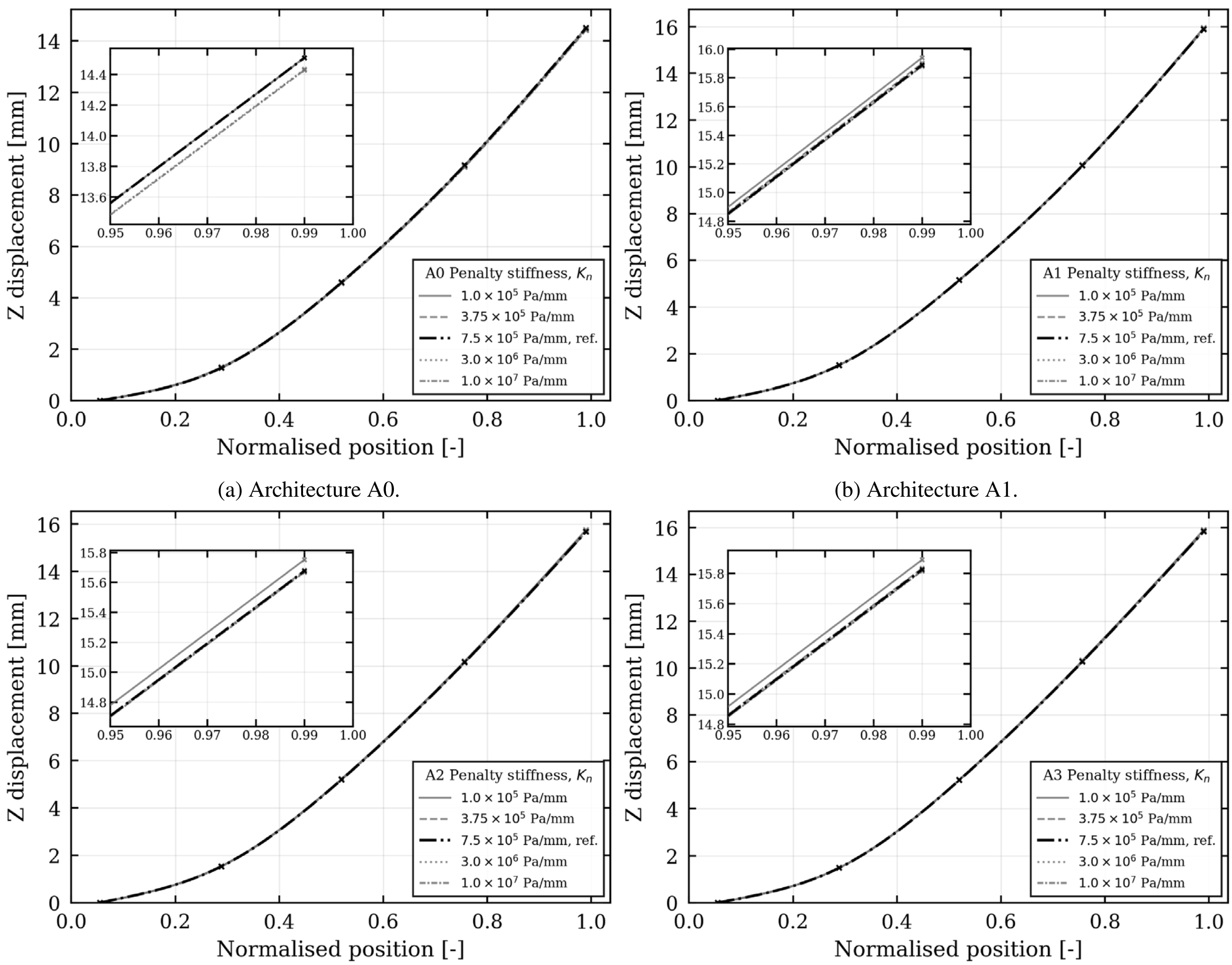

(a) Architecture A0.

(b) Architecture A1.

(c) Architecture A2.

(d) Architecture A3.

Fig. 15. Sensitivity of the predicted spanwise deflection profiles to the platelet-to-platelet cohesive stiffness, k_i^0, for the tested architectures.

changes, instrumental displacement uncertainty, and numerical sensitivity analyses. This limitation is evident when comparing small differences between architectures, such as the δ_V displacement difference between A1 and A3. Accordingly, the following discussion focuses on architecture-dependent trends and their consistency with the numerical model and expected load-transfer mechanisms rather than on statistical significance.

A key question posed in this study was whether the additional architectural variables unique to woven platelet systems could be meaningfully perceived at the component scale. The experimental results supports this. The clearest comparison is between A1 and A2, which vary in platelet width and transverse superposition. Across the measured span, A1 exhibits lower deflection values than A2. The wider platelets and greater transverse overlap in A1 reduce the number of transverse platelet edges across the shell width while improving the continuity of the transverse load-transfer path. This reduces the number of locations where σ_{22}, σ_{23}, and σ_{33} must be locally re-equilibrated, while also reducing perturbations to the longitudinal bending load path governed by σ_{11} and σ_{13}.

The A2–A3 comparison isolates the effect of transverse superposition for a given platelet width. Increasing δ_w from 25% to 50% increases the bonded area available for shear transfer while also providing a larger region over which σ_{22} and σ_{23} can develop and equilibrate, reducing the severity of interlaminar stress concentrations at platelet edges. The lower deflection of A3 relative to A2 is consistent with improved load continuity through the overlap network and is aligned with the expected behaviour of woven EPPs, where reduced overlaps increase the number of effective platelet edges while creating smaller critical bonded regions over which stress-transfer and interlaminar shear stresses can be equilibrated.

The comparison between A1 and A3 isolates the effect of platelet width for a given transverse superposition. Although A3 measured a lower displacement value at the outermost transducer location, δ_V, A1 exhibits lower deflection values over the preceding spanwise measurement locations. This comparison, in light of the previous architectures, suggests that platelet width and transverse superposition act through different but coupled mechanisms. Wider platelets reduce the number of transverse discontinuities within the stress transfer network, while larger transverse superposition increases the smallest bonded area available for each transverse overlap where interlaminar shear stresses must be re-equilibrated. For A1–A3, the wider platelets control the relative spatial positioning of the transverse incisions and resulting overlap regions, both minimising perturbations to the axial stress and resulting in a greater overlap length for re-equilibrating interlaminar stresses. As such, wider platelets would be expected to improve stiffness retention, as observed from δ_{II}–δ_{IV}.

A further modelling idealisation concerns the treatment of the incisions between adjacent platelets, Δ_s. In the FE model, these regions were represented as 100 μm void spaces in order to preserve a clear geometric discontinuity while ensuring that platelet-to-platelet load transfer occurred through the prescribed cohesive interfaces. However, in the manufactured components, resin flow during consolidation is expected to fill these incisions, forming resin-rich regions [38]. Although the dominant load-transfer mechanism in discontinuous platelet systems remains governed by interlaminar shear and peel stresses across the overlapping interfaces, resin-rich material within the discontinuities would still provide a secondary stiffness contribution through partial bridging of adjacent platelet edges. Neglecting this contributions removes a possible load-transfer path, however minimal it could be, and may underestimate the effective stiffness of the discontinuous network. This incision idealisation could be a possible source of overestimation of the measured deflection for the computational model. The effect is expected to primarily influence the absolute compliance level rather than the relative architecture-dependent trends, as the incision idealisation was applied to all EPP architectures.

The transferability of the platelet-array model is attributed to its explicit representation of the dominant meso-scale geometric features, including platelet dimensions, overlap topology, and platelet-to-platelet interfaces. These features govern load redistribution in the present linear-elastic stiffness analysis. However, the model homogenises finer woven-fabric characteristics such as tow heterogeneity, tow undulation, and crimp. Therefore, extension towards damage initiation, progressive failure, or post-elastic response for woven platelet laminates would require a more detailed formulation.

The numerical offsets discussed in Section 3.2 may arise from a combination of modelling based idealisations and experimental sensitivities. The idealised encastre boundary condition and coupling-based load introduction adopted in the FE model do not explicitly account for potential compliance contributions from the mounting hardware, adhesives, and fasteners or local contact conditions that were present in the physical test setup. In addition, the contact displacement transducers are sensitive to probe alignment, local surface normal variations, and the evolution of the contact point during bending. These effects are expected to be amplified towards the free end, where both displacement magnitude and local rotation are greatest.

The agreement between the predicted and measured responses indicates that the dominant stiffness-governing mechanisms are captured by the present modelling strategy. These results support two central conclusions. First, woven EPP architectures can preserve a large proportion of continuous-laminate stiffness, even when implemented in an unoptimised closed-section component. Second, the additional architectural variables unique to woven platelets, namely platelet width and transverse superposition, influence the stiffness of the structural component through their effect on transverse discontinuity density, bonded overlap area, and the resulting three-dimensional inter-platelet shear-transfer network. These effects can be resolved using an adapted platelet-array FEM within the linear-elastic regime.

5. Conclusions

This work investigated the linear elastic stiffness response of woven EPP laminates in a closed-section component-level geometry and assessed the capability of a platelet-based FE framework to predict the corresponding structural response. Three tailored EPP architectures with controlled and repeatable discontinuity patterns were manufactured and benchmarked against an equivalent continuous laminate baseline geometry.

Experimentally, the introduction of platelet discontinuities reduced the effective bending stiffness relative to the continuous baseline laminate. Despite this stiffness penalty, the spanwise deflection profiles for all configurations remained similar in shape, showcasing a consistent bending-dominated deformation mode across all laminates. Comparisons between the EPP architectures indicated that transverse architectural variables influence stiffness retention for a closed-section structure. For a linear-elastic loading regime, platelet width and transverse superposition affect the stress-transfer network's efficiency, by altering the density of transverse discontinuities and the available bonded overlap area.

A UD-derived linear-elastic FEM framework was implemented to reproduce the experimental deflection trends with good agreement. Averaged across the transducer measurement locations, the mean differences between the experimental and numerical displacements were 2.92% for the continuous baseline (A0), 5.33% for EPP architecture A1, 0.82% for EPP architecture A2, and 4.90% for EPP architecture A3, with limited scatter for the last two architectures. The model captured the observed bending-dominated deformation shape and supports the applicability of platelet-based modelling approaches to woven EPP systems under elastic loading conditions.

Overall, these findings demonstrate that woven EPP architectures can be tailored to preserve a substantial fraction of baseline stiffness while enabling repeatable meso-structural control. This strengthens the case for high-value reuse of woven prepreg offcuts in structurally relevant applications. The validated modelling framework provides a practical platform for future parametric studies quantifying the influence of platelet dimensions, overlap parameters, and stacking sequences on stiffness retention and load transfer, and for identifying architecture-driven stress concentrations that define stiffness-efficiency design envelopes for closed-section structures.

Nomenclature

BaM	Brick-and-Mortar
CFRP	Carbon Fibre Reinforced Polymer
DCFC	Discontinuous Carbon Fibre Composites
DoE	Design of Experiments
δl	Platelet length superposition
δw	Platelet width superposition
δ_i	Transducer displacement location
E	Young's Modulus
EPP	Engineered Prepreg Platelets
FE	Finite element
FEM	Finite element modelling
k_i^0	Initial cohesive stiffness
l_p	Platelet length
w_p	Platelet width
n_p	Number of plies
PPMC	Prepreg Platelet Moulded Composite
QI	Quasi-isotropic
SF	Short fibre
t_p	Ply thickness
UD	Unidirectional

CRediT authorship contribution statement

Alessandro Masetti Placci: Writing – review & editing, Writing – original draft, Visualization, Validation, Project administration, Methodology, Investigation, Formal analysis, Data curation, Conceptualization. **Luca Bernini:** Writing – review & editing, Supervision. **Paolo Albertelli:** Writing – review & editing, Supervision.

Declaration of competing interest

The authors declare the following financial interests/personal relationships which may be considered as potential competing interests: Alessandro Masetti Placci reports financial support was provided by Racing Bulls S.p.A. Alessandro Masetti Placci reports a relationship with Racing Bulls S.p.A. that includes: consulting or advisory. If there are other authors, they declare that they have no known competing financial interests or personal relationships that could have appeared to influence the work reported in this paper.

Acknowledgements

Project funded under the National Recovery and Resilience Plan (NRRP), Mission 04 Component 2 Investment 1.5—NextGenerationEU, Call for tender n. 3277 dated 30 December 2021 Award Number: 0001052 dated 23 June 2022. The authors would like to thank Racing Bulls S.p.A. Formula One Team for manufacturing the specimens, providing the testing apparatus, and their industrial knowledge and experience in composites manufacturing.

Data availability

Data will be made available on request.

References

[1] Masetti Placci A, Bernini L, Albertelli P, Cimino C, Perotti F, Monno M. A review on circular economy approaches for pre-impregnated carbon composites mould remanufacturing. Int J Precis Eng Manuf.-Green Technol 2025. http://dx.doi.org/10.1007/s40684-025-00776-3.

[2] Montagna LS, de Melo Morgado GF, Lemes AP, Passador FR, Rezende MC. Recycling of carbon fiber-reinforced thermoplastic and thermoset composites: A review. J Thermoplast Compos Mater 2022;36:3455–80. http://dx.doi.org/10.1177/08927057221108912.

[3] Sloan J. The outlook for carbon fiber supply and demand. 2025, URL: https://www.compositesworld.com/articles/the-outlook-for-carbon-fiber-supply-and-demand.

[4] Zhang J, Chevali VS, Wang H, Wang C-H. Current status of carbon fibre and carbon fibre composites recycling. Composites B 2020;193:1–15. http://dx.doi.org/10.1016/j.compositesb.2020.108053.

[5] Nilakantan G, Nutt S. Reuse and upcycling of thermoset prepreg scrap: Case study with out-of-autoclave carbon fiber/epoxy prepreg. J Compos Mater 2017;52(3):341–60. http://dx.doi.org/10.1177/0021998317707253.

[6] Alves M, Pimenta S. The influence of 3D microstructural features on the elastic behaviour of tow-based discontinuous composites. Compos Struct 2020;251:112484. http://dx.doi.org/10.1016/j.compstruct.2020.112484.

[7] Wan Y, Takahashi J. Tensile and compressive properties of chopped carbon fiber tapes reinforced thermoplastics with different fiber lengths and molding pressures. Composites A 2016;87:271–81. http://dx.doi.org/10.1016/j.compositesa.2016.05.005.

[8] Kravchenko SG, Sommer DE, Pipes RB. Uniaxial strength of a composite array of overlaid and aligned prepreg platelets. Composites A 2018;109:31–47. http://dx.doi.org/10.1016/j.compositesa.2018.02.032.

[9] Sommer DE, Kravchenko SG, Pipes RB. Investigation of the notch sensitivity of tailorable long fiber discontinuous prepreg composite laminates. Composites A 2025;188:108508. http://dx.doi.org/10.1016/j.compositesa.2024.108508.

[10] Feraboli P, Peitso E, Deleo F, Cleveland T, Stickler PB. Characterization of prepreg-based discontinuous carbon fiber/epoxy systems. J Reinf Plast Compos 2008;28(10):1191–214. http://dx.doi.org/10.1177/0731684408088883.

[11] Milite A, Frassine R, Krajangsawasdi N, Longana ML. Management strategies for uncured thermoset and thermoplastic prepreg waste: A review. Composites B 2026;313:113402. http://dx.doi.org/10.1016/j.compositesb.2026.113402.

[12] Wan Y, Takahashi J. Tensile properties and aspect ratio simulation of transversely isotropic discontinuous carbon fiber reinforced thermoplastics. Compos Sci Technol 2016;137:167—-176. http://dx.doi.org/10.1016/j.compscitech.2016.10.024.

[13] Aranke SS, Pipes RB. Platelet critical length for prepreg platelet molded composites. Composites A 2024;181:108142. http://dx.doi.org/10.1016/j.compositesa.2024.108142.

[14] Pimenta S, Robinson P. An analytical shear-lag model for composites with 'brick-and-mortar' architecture considering non-linear matrix response and failure. Compos Sci Technol 2014;104:111–24. http://dx.doi.org/10.1016/j.compscitech.2014.09.001.

[15] Wyser Y, Leterrier Y, Månson J-AE. Analysis of failure mechanisms in platelet-reinforced composites. J Mater Sci 2001;36(7):1641–51. http://dx.doi.org/10.1023/a:1017583432728.

[16] Yamashita S, Hashimoto K, Suganuma H, Takahashi J. Experimental characterization of the tensile failure mode of ultra-thin chopped carbon fiber tape-reinforced thermoplastics. J Reinf Plast Compos 2016;35(18):1342–52. http://dx.doi.org/10.1177/0731684416651134.

[17] Ko S, Yang J, Tuttle ME, Salviato M. Effect of the platelet size on the fracturing behavior and size effect of discontinuous fiber composite structures. Compos Struct 2019;227:1–13. http://dx.doi.org/10.1016/j.compstruct.2019.111245.

[18] Lakes R. Materials with structural hierarchy. Nature 1993;361(6412):511–5. http://dx.doi.org/10.1038/361511a0.

[19] Katsivalis I, Persson M, Johansen M, Moreau F, Kullgren E, Norrby M, Zenkert D, Pimenta S, Asp LE. Strength analysis and failure prediction of thin tow-based discontinuous composites. Compos Sci Technol 2024;245:110342. http://dx.doi.org/10.1016/j.compscitech.2023.110342.

[20] Kravchenko SG, Sommer DE, Denos BR, Avery WB, Pipes RB. Structure-property relationship for a prepreg platelet molded composite with engineered meso-morphology. Compos Struct 2019;210:430–45. http://dx.doi.org/10.1016/j.compstruct.2018.11.058, URL: https://doi.org/10.1016/j.compstruct.2018.11.058.

[21] Taketa I, Okabe T, Kitano A. A new compression-molding approach using unidirectionally arrayed chopped strands. Composites A 2008;39(12):1884–90. http://dx.doi.org/10.1016/j.compositesa.2008.09.012.

[22] Aitharaju V, Averill R. Three-dimensional properties of woven-fabric composites. Compos Sci Technol 1999;59(12):1901–11. http://dx.doi.org/10.1016/s0266-3538(99)00049-4.

[23] Chowdhury IR, Summerscales J. Woven fabrics for composite reinforcement: A review. J Compos Sci 2024;8(7):280. http://dx.doi.org/10.3390/jcs8070280.

[24] Ashby MF. Materials Selection in Mechanical Design. London: Butterworth-Heinemann; 2025, p. 600.

[25] RB VC. Visa Cashapp RB racing bulls F1 team. 2024, URL: https://www.visacashapprb.com/en/.

[26] CIT. CIT composite materials Italy. 2024, URL: https://www.composite-materials.it/pagina.php.

[27] Industries E. High-performance foam cores for sandwich structures ROHACELL. 2024, URL: https://composites.evonik.com/en/products-services/foams/rohacell.

[28] 3M. 3M™ Scotch-Weld™ structural epoxy adhesive EC-9323 B/A. 2025, URL: https://www.3mitalia.it/3M/it_IT/p/d/v000118253/.

[29] Corp. NI. LabVIEW. 2025, URL: https://www.ni.com/it-it/shop/product/labview.html.

[30] Transducers A. Displacement transducers: LDT_AMP. 2025, URL: https://www.aep.it/en/product/displacement-transducers/ldt-amp/.

[31] Pipes RB, Pagano N. Interlaminar stresses in composite laminates under uniform axial extension. J Compos Mater 1970;4(4):538–48. http://dx.doi.org/10.1177/002199837000400409.

[32] L. J. H-S. Adhesive-Bonded Single-Lap Joints. NASA; 1973, p. 116, URL: https://ntrs.nasa.gov/citations/19740005083.

[33] Systèmes D. Abaqus documentation. Providence, RI: Dassault Systèmes; 2023.

[34] Altair Engineering I. Altair hyperMesh. Troy, MI, USA: Altair Engineering, Inc.; 2024.

[35] Meng X, Zhuo P, Li S, Yan Y, Yan S. A simple off-axis tension method for shear characterization of woven composites derived from material symmetry analysis. Compos Sci Technol 2026;282:111672. http://dx.doi.org/10.1016/j.compscitech.2026.111672.

[36] Zou Z, Reid SR, Li S, Soden PD. Modelling interlaminar and intralaminar damage in filament-wound pipes under quasi-static indentation. J Compos Mater 2002;36(4):477–99. http://dx.doi.org/10.1177/0021998302036004539.

[37] Ko S, Nakagawa T, Chen Z, Avery WB, Adams EJ, Soja MR, Larson MH, Park CY, Yang J, Salviato M. Effects of average number of platelets through the thickness and platelet width on the mechanical properties of discontinuous fiber composites. Composites A 2024;177:107945. http://dx.doi.org/10.1016/j.compositesa.2023.107945.

[38] Blest D, McKee S, Zulkifle A, Marshall P. Curing simulation by autoclave resin infusion. Compos Sci Technol 1999;59(16):2297–313. http://dx.doi.org/10.1016/s0266-3538(99)00084-6.